NANO LETTERS

Letter

pubs.acs.org/NanoLett

Nonlinear Raman Effects Enhanced by Surface Plasmon Excitation in Planar Refractory Nanoantennas

Sergey S. Kharintsev,*[,†,‡] Anton V. Kharitonov,[†] Semion K. Saikin,[§,∥] Alexander M. Alekseev,[⊥,#] and Sergei G. Kazarian[○]

[†]Department of Optics and Nanophotonics, Institute of Physics, Kazan Federal University, Kremlevskaya, 16, Kazan 420008, Russia

[‡]Institute of Perspective Technologies, Tatarstan Academy of Sciences, Baumana, 20, Kazan 420111, Russia

[§]Department of Chemistry and Chemical Biology, Harvard University, 12 Oxford Street, Cambridge, Massachusetts 02138, United States

[∥]Department of Theoretical Physics, Institute of Physics, Kazan Federal University, Kremlevskaya, 16, Kazan 420008, Russia

[⊥]National Laboratory Astana, Nazarbayev University, Kabanbay batyr Avenue, 53, Astana 01000, Kazakhstan

[#]STC NMST, Moscow Institute for Electronic Technology, Moscow 124498, Russia

[○]Department of Chemical Engineering, Imperial College London, South Kensington Campus, London SW7 2AZ, United Kingdom

ABSTRACT: We consider a nonlinear mechanism of localized light inelastic scattering within nanopatterned plasmonic and Raman-active titanium nitride (TiN) thin films exposed to continuous-wave (cw) modest-power laser light. Owing to the strong third-order nonlinear interaction between optically excited broadband surface plasmons and localized Stokes and anti-Stokes waves, both stimulated and inverse Raman effects can be observed. We provide experimental evidence for coherent amplification of the localized Raman signals using a planar square-shaped refractory antenna.

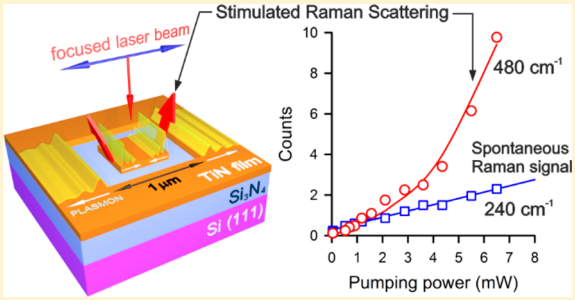

KEYWORDS: *Nonlinear refractory plasmonics, planar antenna, titanium nitride, stimulated Raman scattering, inverse Raman effect, tip-enhanced Raman scattering*

Enhancement and localization of nonlinear optical effects due to surface plasmon-polariton (SPP) excitation in confined metallic nanostructures routes toward the development of ultracompact coherent light sources[1,2] and single-molecule-sensitive detectors.[3,4] Strong electric fields of 10^7−10^9 V/m can be produced in nanostructures exposed to cw modest-power laser pump and, as a corollary, the second- and third-order optical nonlinearities become substantial.[5] This means that nonlinear phenomena such as the stimulated Raman effect, inverse Raman effect, and coherent anti-Stokes Raman scattering could potentially appear in these nanostructures, which is in analogy to bulk matter exposed to high-power laser pulses.[6−10] In contrast to the spontaneous Raman scattering, which is used as an analytical tool for molecular recognition, SPP-enhanced coherent nonlinear Raman processes can be used for an amplification of confined optical signals.

Despite considerable progress towards nonlinear plasmonics over the past decade,[11,12] mitigating the huge ohmic losses in plasmonic nanostructures is still a principle challenge.[13] Normally, nanostructures such as stripes and waveguides are supported with gain media to compensate these losses.[14,15] Such sandwich-like planar interfaces cannot provide an efficient plasmon−phonon coupling because of the exponential attenuation of SPPs toward the direction perpendicular to the contact plane. To improve the performance of optical signal amplification (or attenuation) due to a bulk effect, the planar antenna should possess simultaneously plasmonic and optical gain (or loss) properties. Well-established noble metals, such as gold and silver, are not Raman-active media. However, these materials experience a sufficient photoinduced thermal damage at high electrical fields that are required for observation of nonlinear effects.[16] Recently, Shalaev's group proposed the use of a refractory plasmonic material, titanium nitride (TiN), which has a high melting point of 2930 °C.[17] Epitaxially grown TiN thin films show a high value of figure-of-merit (FOM) to excite the SPPs which is comparable to the FOM for gold.[18] Moreover, this material has tunable optical properties and high hardness.[13,19] Unlike noble metals, TiN can sustain high temperatures and exhibits large optical nonlinearities.[16] As of today, the third-order susceptibility $\chi^{(3)}$ of a crystalline TiN thin film reaches up to $\chi^{(3)} = -(5.3 + 0.2i) \times 10^{-18}$ [m^2/V^2], as experimentally demonstrated by Boltasseva's group.[20] Among other nonlinear materials,[21] the high value of $\chi^{(3)}$ for TiN makes this material attractive for nonlinear optical interactions.

Received: May 28, 2017
Revised: August 10, 2017
Published: August 16, 2017

DOI: 10.1021/acs.nanolett.7b02252
Nano Lett. 2017, 17, 5533−5539

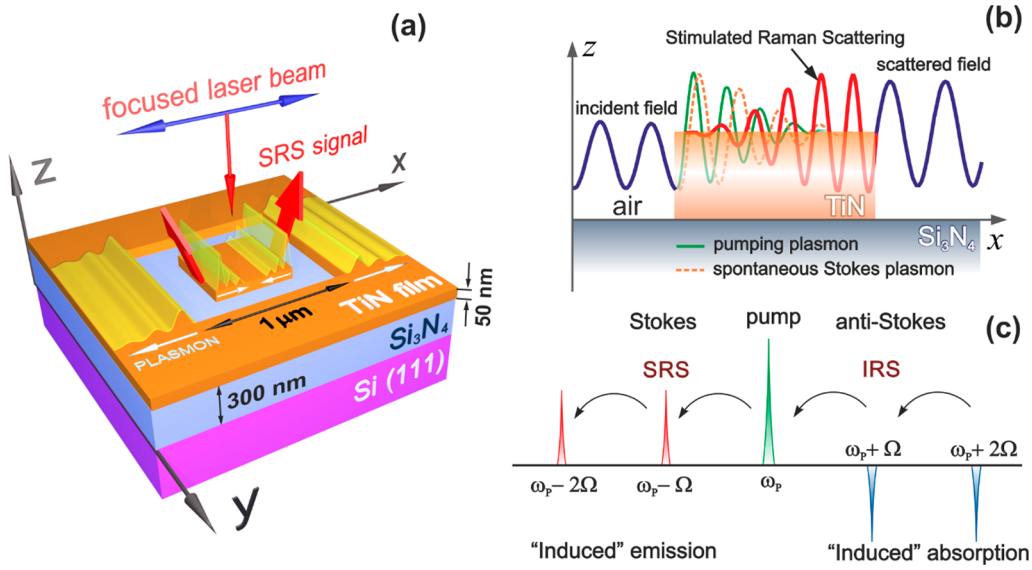

Figure 1. (a) Schematic circuit of a square grooved TiN thin film, (b) demonstration of the SRS effect within the TiN antenna, (c) illustration of SRS and IRS effects.

A specific feature of TiN is its Raman activity. Although the first-order Raman scattering is forbidden due to the symmetry of a NaCl-type cubic lattice, the presence of structural defects, even in stoichiometric TiN substances, provides access to the first-order acoustic and optical modes.[22−24]

In this Letter, we experimentally demonstrate SPP-enhanced stimulated Raman (gain) emission and indirect signatures of (loss) absorption effects (referred to as stimulated Raman scattering (SRS) and inverse Raman scattering (IRS), respectively[6,7,9]) using a square shaped nonresonant antenna engraved on a TiN thin film. Our study provides the understanding of enhancement effects of localized Raman light due to the nonlinear interaction of plasmon−phonon modes through the $\chi_R^{(3)}$ coupling mechanism.

Figure 1a shows a schematic circuit of a square-shaped TiN antenna fabricated on a 50 nm TiN thin film by focused ion beam milling. The planar antenna sizes were 100, 200, 300, 400, and 500 nm. The TiN thin film was deposited on a 300 nm thick Si_3N_4 film by direct current (dc) reactive magnetron sputtering in an argon−nitrogen environment at elevated temperature of 380 °C.

The optical properties of the TiN thin films prepared at different ratios of Ar/N_2 were characterized with spectroscopic ellipsometry (UVISEL 2 Horiba, Japan). Figure 2 demonstrates real and imaginary parts of dielectric permittivity of the TiN films that were fitted with the Drude-Lorentz model. As seen from the figure, all films can potentially be plasmonic at wavelengths above 480 nm. In our experiments, we used the TiN film sputtered at Ar/N_2 = 50:50.

All optical and spectroscopic measurements were performed with a multipurpose analytical system NTEGRA SPECTRA (NT-MDT, Russia). The raster scanned antennas were exposed to a 632.8 nm linearly polarized fundamental Gaussian beam that was focused with a 100× objective (N.A. = 0.7) in epiconfiguration. The laser power was about 1 mW corresponding to the intensity of about 1 MW/cm^2. Raman maps of 128 × 128 pixel were captured with an electron multiplying charge coupled device detector (Andor, U.K.) cooled down to −100 °C. The exposure time was 10 ms per a pixel. The laser beam was coupled to a cone-shaped gold tip to

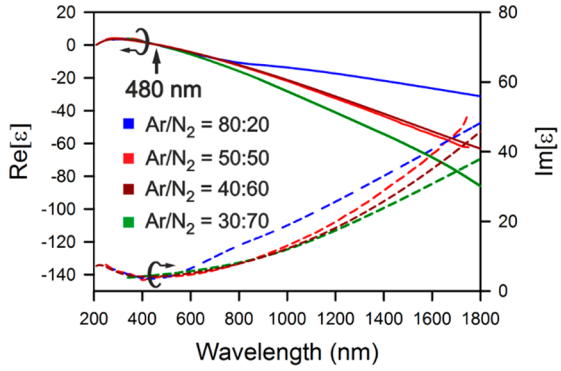

Figure 2. Real and imaginary parts of the dielectric permittivity of the TiN thin film sputtered at different ratio of Ar/N_2 as functions of the wavelength.

perform tip-enhanced Raman scattering (TERS) measurements. This tip was designed using the dc-pulsed electrochemical etching with the self-tuned duty cycle.[25] Its curvature radius was estimated to be about 28 nm. A tip−sample distance was controlled by the normal force mechanism because a tuning fork sensor equipped with the gold tip was oriented almost parallel to the antenna plane. Because the tip was positioned between the objective and the sample, the tip shaft was manually bent to an angle of 52° that allowed the light to get focused onto the tip apex.

A planar square-shaped TiN antenna can be considered as a system consisting of two edge-like optical nanoantennas coupled by a subwavelength waveguide. The antenna edges are fused due to the ion beam milling and their curvature radii reach about 25 nm. The edge-nanoantennas convert TM-polarized far-field optical waves to localized surface plasmons. For short enough waveguides, the optical near-fields excite counter-propagating coherent SPPs forming TM-polarized standing-wave resonances at specific widths of the antenna. The incident electromagnetic wave can be enhanced by feeding it with the edge plasmonic nanoantenna and a constructive interference of the pump with their reflections in the Fabry-Pérot resonator.[26,27]

DOI: 10.1021/acs.nanolett.7b02252
Nano Lett. 2017, 17, 5533−5539

We assume that all plasmon waves propagate in the x-direction. The associated electric fields have the following form

$$\mathbf{E}(x, z, t) = A(x, z)e^{i(kx-\omega t)} + c{\cdot}c \quad (1)$$

where $k = 2\pi c/\omega_0\sqrt{\varepsilon(\omega)\varepsilon_e/(\varepsilon(\omega) + \varepsilon_e)}$ is an x-projection of the complex wavevector $\boldsymbol{k}$, c is the light speed in vacuum, ω is a frequency of the light wave, $A(x,z)$ is the field amplitude, and $\varepsilon(\omega)$ and ε_e are the permittivity of the antenna and an environment, respectively. Because the wavevector $\boldsymbol{k}$ is complex in the metallic resonator, the electromagnetic wave, defined by eq 1, is damped and localized. Thus, we distinguish local optical fields $\mathbf{E}$ or internal intensities I inside the antenna from their counterparts $\mathbf{E}_0$ and I_0 outside. They relate as $\mathbf{E} = g\mathbf{E}_0$ and $I = g^2I_0$, where g is a field-enhancement factor, $I_0 = c\varepsilon_0 n_e|E_0|^2$ (ε_0 is the dielectric permittivity in vacuum).

The enhancement of the pump field $\mathbf{E}_P = A_P e^{i(k_P x - \omega_P t)}$ at different frequencies can be performed using Raman-gain media. Spontaneous Raman scattering generates red-shifted Stokes $\mathbf{E}_S = A_S e^{i(k_S x - \omega_S t)}$ and blue-shifted anti-Stokes $\mathbf{E}_{aS} = A_{aS}e^{i(k_{aS}x - \omega_{aS}t)}$ waves in the TiN film.[22,23] In a cubic nonlinear medium, the two waves with frequencies ω_P and ω_S interact with each other provided that $\omega_P - \omega_S \approx \Omega$ or $\omega_P - \omega_{aS} \approx -\Omega$ (Ω is a phonon frequency) and their amplitudes A_P and A_S are comparable. The coupling of the two localized plasmonic waves through modulating the third-order Raman susceptibility $\chi_R^{(3)}$ creates an ensemble of coherently driven vibrational modes. The real and the imaginary parts of $\chi_R^{(3)}$ describe a Raman phase shift and a Raman gain, respectively. Figure 1b depicts schematically a stimulated Raman scattering mechanism in the TiN antenna. A nonlinear interaction of the fast-damping plasmonic pump and spontaneous Stokes wave yields a stimulated Raman response, which can be converted into the far-field with the edge-like nanoantenna.

In the SRS regime, the pump intensity decreases due to the energy transfer to the Stokes wave. About half of the total energy can potentially be converted to one of the strongest Stokes waves, for example, the first-order Raman band. As a result, this band serves as a secondary source to excite the second, the third and so on overtones $\omega_P - 2\Omega$, $\omega_P - 3\Omega$, as shown in Figure 1c. Importantly, the energy is transferred into vibrational modes at multiple frequencies, in other words, no anharmonicity of vibrations are observed.[6,7] SRS weakens when a background vibrational level is depleted and eventually this effect disappears. Moreover, it leads to the inverse population and thus the up-conversion efficiency increases. The $\chi_R^{(3)}$ nonlinear interaction between the broadband plasmon pump and the anti-Stokes wave can result in the depletion of anti-Stokes photons due to inverse Raman scattering (IRS).[6,9] Figure 1c schematically shows both the "induced" emission and the "induced" absorption mechanisms. A cascade energy transfer from the anti-Stokes region to the Stokes region, as shown in Figure 1c with arrows, amplifies the pump intensity. In reality, the total intensity at the pump frequency is determined by a balance of the competitive contributions, SRS and IRS.

The Stokes wave amplitude A_S is driven by the nonlinear propagation equation[6]

$$\frac{\partial A_S}{\partial x} = g^2\frac{3i\chi_R^{(3)}(\omega_S)}{n_S c}\omega_S A_S|A_P|^2 \quad (2)$$

where n_{+S} is a refractive index for the Stokes wave at a specific frequency ω_S. As seen from eq 2, the phase matching condition for the SRS effect is automatically fulfilled, since $\Delta k = k_S - k_S = 0$. Eq 2 describes changes in the amplitude due to the modulation of $\chi_R^{(3)}$ rather than the damping of the plasmon pump. In the nondepleted pump approximation, when $|A_P|^2 \approx$ const, eq 2 demonstrates the exponential growth of the Stokes wave amplitude. In the SRS regime we have $|A_P|^2 + |A_S|^2 =$ const. With that, a solution of eq 2 can be readily derived:

$$A_S(x) = A_S(0)(1 + e^{-2x/d})^{-1/2} \quad (3)$$

where $d = -in_S c/(3g^2\omega_S\chi_R^{(3)})$ is an exponential decay length. By introducing the Raman gain χ_R and the attenuation of the Stokes plasmon α, defined as $\chi_R(\omega_S) = -3\omega_S g^2\,\mathrm{Im}[\chi_R^{(3)}]/(n_S n_P \varepsilon_0 c^2)$ and $\alpha = 2n_S c\varepsilon_0/l_{pl}$ (where $l_{pl} = (2\,\mathrm{Im}[k])^{-1}$ is the energy attenuation length), we can write a differential equation for the internal intensity of the Stokes wave as follows

$$\frac{\partial I_S}{\partial x} = [\chi_R I_S I_P - \alpha I_S]e^{-x/l_{pl}} \quad (4)$$

Extra enhancement can be achieved using the Fabry-Pérot resonator where the pump and the Stokes waves are resonant.[14,15,27−29] This means that they propagate many times back and forth within the antenna. The contribution into the field enhancement due to the resonant Raman-active medium is described by the total phase shift $\Delta\phi_{tot}$ accumulated during the roundtrip of the plasmon wave, eq 5

$$\Delta\phi_{tot} = N\frac{2\pi}{\lambda_{eff}}L = \Delta\phi_{exc} + \Delta\phi_{refl} + 2\Delta\phi_R \quad (5)$$

where N is an integer number, L is a linear size of the antenna, $\lambda_{eff} = p_1 + p_2[\lambda/\lambda_p]$ is the effective wavelength, where λ_p is the plasma wavelength of the metal, and p_1 and p_2 are constants depending on the geometry and the dielectric permittivity of the resonator.[30] The Raman phase shift $\Delta\phi_R$ for the Stokes wave is defined as $\Delta\phi_R(x) \sim \mathrm{Re}[\chi_R^{(3)}]I_P x$. The phase shift upon the excitation of a localized plasmon at the edges reads as $\Delta\phi_{exc} = \arctan[2\Gamma\omega/(\omega_{pl}^2 - \omega^2)]$, where Γ is a damping constant and ω_{pl} is a plasmon resonance frequency.[15] Thus, the resonator itself can enhance the internal intensities I_P and I_S by a factor $M_l = (1 - R_1^l)(1 + R_2^l)/(1 - \sqrt{R_1^l R_2^l})^2$ (R_1^l and R_2^l are reflectivity for the two sides, $l = P$ or S). However, the prolongation of the optical path with a high-finesse doubly resonator fails for both the SPP pump and the SPP Stokes waves because of a strong mismatch of spatial frequencies k_P and k_S.[31] Depending upon the excitation wavelength, the enhancement factor, M_l, may vary within the range of 2−4.

Numerical simulations of the optical reflection $R(\lambda)$ normalized per antenna area S as a function of an excitation wavelength and the antenna size are shown in Figure 3. Calculations of $R(\lambda) = \int \mathrm{Re}[\boldsymbol{P}(\lambda)]\boldsymbol{n}\,d\sigma/2W(\lambda)$ (where $\boldsymbol{P}(\lambda)$ is the Poynting vector, $\boldsymbol{n}$ is a normal unit vector corresponding to the orientation of an elementary area $d\sigma$, $W(\lambda)$ is a total power of the incident irradiation) were performed using the finite difference time domain method (Lumerical FDTD software package). From Figure 3a, we see that the 500 × 500 nm^2 planar antenna is able to effectively scatter the incident light due to the localized plasmon resonances that occur within the spectral range of 600−900 nm. However, this structure allows us to minimize a contribution from the Fabry-Pérot resonances into the field enhancement and, thus, focus on the nonlinear Raman enhancement only. As follows from Figure 3b, a 632.8

DOI: 10.1021/acs.nanolett.7b02252
Nano Lett. 2017, 17, 5533−5539

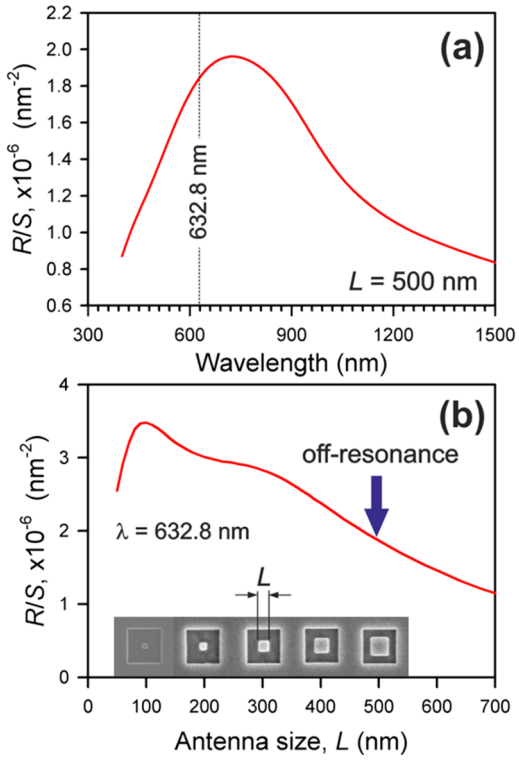

Figure 3. Calculated optical reflection R normalized per antenna area S versus excitation wavelength (a) and antenna size (b) for the 500 × 500 nm^2 planar antenna and 632.8 nm excitation wavelength, respectively. Inset in (b) shows SEM images of the planar TiN antennas of different sizes L.

nm laser field excites standing SPP waves in planar antennas with L_1 = 110 nm and L_2 = 310 nm only.

Figure 4a,b demonstrates a SEM image of a 500 × 500 nm^2 planar antenna and far-field Raman spectra taken at spots marked with a circle and a square in Figure 4c, respectively. In the vicinity of the edges, we observe the extraordinary amplification of a Raman peak at 480 cm^{-1} (a circle). Whereas, far from the antenna the Raman peaks become weak because of high reflectivity R (for example, R = 0.412 at 780 nm[20]) for TiN and film thickness of tens of nanometers. The edgelike optical nanoantennas feed the incident illumination and convert it to a localized plasmonic mode to further excite coherent SPPs on both sides of the antenna. At the central part of the structure, we observe a relatively small enhancement due to the diffraction-limited Raman signals from the edges. The line width of the 480 cm^{-1} band, which equals about 50 cm^{-1}, is caused by a short lifetime of SPPs, that is, on the order of tens of femtoseconds, and as a consequence the SPP propagation length $l_{pl} \sim 1$ μm.

We claim that this field enhancement is directly related to the SPP excitation. To verify this hypothesis, we measured Raman maps of the antenna for two linear polarizations that are mutually transverse (Figure 4c,d). An observable polarization dependence gives convincing evidence for SPP excitation on the resonator edges. The edge-enhanced Raman spectrum is accompanied by fluorescence of TiN that ranges from 2.1 to 3.4 eV.[32] Structural defects of the crystal lattice, including donor states of the nitrogen vacancies, lead to radiative transitions from localized states within the forbidden band. Localized plasmon gap-modes can be easily visualized with the polarized TERS method. Figure 4e,f demonstrate the TERS maps captured at 480 cm^{-1} that were recorded by raster scanning the planar antenna beneath the gold tip illuminated with the focused laser beam. Nonsymmetric spectroscopic responses for the two linear polarizations are caused by the high surface roughness of the antenna and a nanoantenna tilt of 52° with respect to the surface normal. The near-field polarization

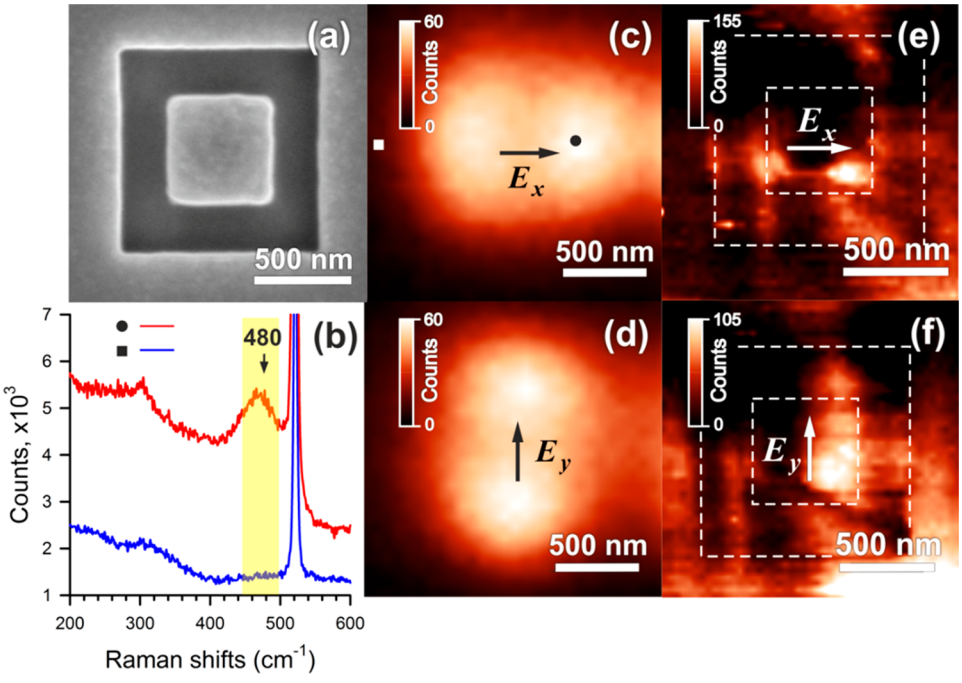

Figure 4. (a) SEM image of a square grooved TiN thin film, (b) Raman spectra captured at two spots marked as a circle and a square in (c); far-field (c,d) and near-field Raman (e,f) maps taken at 480 cm^{-1} for two linear polarizations.

DOI: 10.1021/acs.nanolett.7b02252
Nano Lett. 2017, 17, 5533−5539

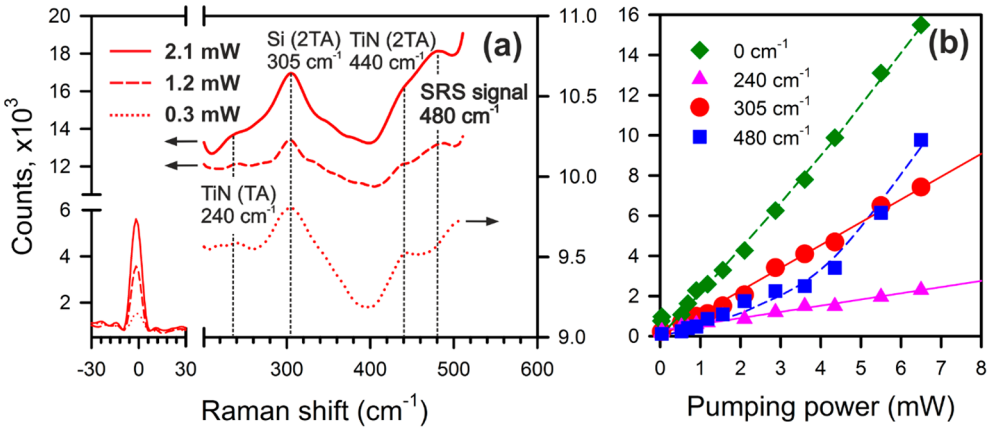

Figure 5. (a) Far-field Raman spectra from the antenna edges at different pumping powers, (b) dependence of the Raman intensity on the pumping power for various spectral peaks.

direction was estimated to be about 47° using the polarization-dependent analysis.[33] On one side of the planar antenna, the gold tip and the edge-nanoantenna form a hot-spot gap in which the field enhancement is maximal. Whereas on the other side, the gap modes are not excited. It is worth to note that the interpretation of the considered TERS maps are ambiguous, because the gold tip acts as both a scattering-type antenna and a plasmonic-type antenna.[34] In addition, the gold tip can be coupled to the edge nanoantenna and, as a consequence, gap modes are excited. In our opinion, the latter contribution dominates the first two when the *p*-polarization of the incident light and the symmetry axis of the tip lie in the same plane (Figure 4e). In the case of the *s*-polarization a dominant contribution to the observable enhancement comes from the SPPs which are elastically scattered with the pointed gold tip (Figure 4f).

Figure 5a shows far-field Raman spectra taken at the edge of the antenna exposed to the focused laser beam with the wavelength of 632.8 nm and different powers of 0.3, 1.2, and 2.1 mW, respectively. The first- and second-order Raman bands with peaks at 240 and 440 cm^{-1} are assigned to a transverse acoustic mode for heavy Ti atoms.[22,35] As follows from the spectrum, the second overtone (2TA) is blue-shifted due to anharmonicity. With the increasing power, we observe an anomalous growth of the Raman peak at 480 cm^{-1} that corresponds to a double wavenumber for the first-order Raman scattering. In Figure 5b, we plot Raman intensity versus the pump power for different vibrational modes of TiN including the excitation wavelength (0 cm^{-1}) and the vibrational mode for Si (2TA) at 305 cm^{-1} as a reference. The scattered intensity at 0 cm^{-1} is attenuated by six orders using two edge-filters. All peaks in Figure 5a are given to scale. A derivative spectrometry technique was used to reveal the net intensities of the studied vibrational modes.[36] Indeed, a linear behavior of the intensity with the pump power was anticipated, as it holds for the reference peak and the first-order Raman peak (Figure 5b). Relative measurement errors for large values of pumping power are roughly 10%, whereas for small pumping power values the errors grow significantly and reach up to 50%. As clearly seen from the latter figure, a nonlinear behavior for the second overtone takes place. These experimental data are well fitted with a cubic function $I_R = aI_0 + bI_0^3$ that describes linear spontaneous and third-order SRS processes. A correlation coefficient, equal to 0.996, confirms the high accuracy of the fitting. If the dependence of the intensity on the pumping power is fitted with a linear function, the correlation coefficient is equal to 0.943. Thus, this is a distinctive signature of the SRS effect. A ratio of the spontaneous and SRS contributions is estimated to be $a/b = 12$. Importantly, the plasmonic Stokes wave interacting with the SPP pump establishes correct phasing of coherent phonons within the lattice. The Raman amplification is produced for any direction of propagation of the Stokes wave.

The strongest SRS signal appears at 480 cm^{-1} that is assigned to the second-order overtone. Because the first-order Raman peak at 240 cm^{-1} is negligible due to the symmetry of a TiN lattice, the energy is mostly transformed to the second-order peak due to the cubic nonlinear mechanism. As known from the theory of SRS,[6] 50% of total pumping is converted into one of the overtones and we observe a giant amplification for one peak only. Other overtones are enhanced as well, as seen in Figure 6 but the enhancement factors are much lower.

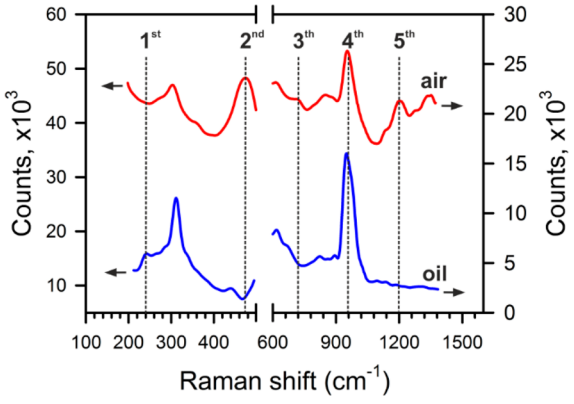

Figure 6. Far-field Raman spectra from the TiN antenna edges for air (red curve) and oil (blue curve) superstrates. Dotted vertical lines indicate positions of the overtones of different orders.

The enhancement factor is defined as EF = $(I_{SERS}/N_{SERS})/(I_{RS}/N_{RS})$, where I_{SERS} and I_{RS} are the intensities of the surface-enhanced Raman scattering (SERS) and spontaneous Raman scattering, respectively, and N_{SERS} and N_{RS} are the number of molecules contributing to the SERS signal and Raman signal, respectively. Assuming that $N_{RS} \sim S = L \times L$ (L is a size of the planar antenna) and $N_{SERS} \sim S_{edge} = \pi\rho L/2$ (ρ is a curvature radius of the antenna edge), we derive the following estimation

DOI: 10.1021/acs.nanolett.7b02252
Nano Lett. 2017, 17, 5533−5539

EF ~ $(I_{SERS}/I_{RS}) \times (L/\rho)$. In our experiment L = 500 nm and ρ = 25 nm, and the EF ~ $20(I_{SERS}/I_{RS})$. From Figure 4b, we can estimate I_{SERS} ~ 1000 (counts) and I_{RS} ~ 50, thus the EF ~ 400. This means that $g = |\mathbf{E}_{loc}|/|\mathbf{E}_{inc}| = 20$, where $\mathbf{E}_{loc}$ and $\mathbf{E}_{inc}$ are the localized and incident electrical fields. It is well-established that the characteristic length for nonlinear optical effects within the bulk materials is estimated to be ~ $\lambda|\mathbf{E}_a|/|\mathbf{E}_{inc}|$ (λ is a wavelength of the incident light and $\mathbf{E}_a \sim 3 \times 10^8$ V/cm is the internal electric field). For nanoscale systems, this estimation should be modified for ~ $\rho|\mathbf{E}_a|/|\mathbf{E}_{loc}|$. Upon illumination of the planar TiN antenna with a focused laser beam using a power of 10 mW (the intensity of $I_0 \sim 3 \times 10^6$ MW/cm^2 or the electric field strength $\mathbf{E}_{inc} \sim 3 \times 10^4$ V/cm), we can readily derive the characteristic length for nanoscale nonlinear effects to be ~125 nm. Finally, this means that stimulated Raman scattering can be observed in our 500 × 500 nm^2 planar TiN antenna.

The presence of higher-order overtones peaked at 720 and 1200 cm^{-1} in the Raman spectra further confirms the SPP-assisted SRS effect, as shown in Figure 6. The fourth overtone at 960 cm^{-1} is not available to observe because of overlapping with the second-order peak of Si. By adding some amount of immersion oil on the same antenna surface, we change a refractive index of the environment for n_e = 1.516. The well-established fact is that plasmon resonances are red-shifted for optically dense superstrates.[31] This means that a Fröhlich criterion fails and SPPs are not excited. Indeed, all overtones disappear in the Raman spectrum displayed as a blue curve in Figure 6. Finally, we can state that the giant amplification of the second-order Raman overtone can be interpreted as the SRS effect.

Figure 5b shows the nonlinear dependence of the Rayleigh line (0 cm^{-1}) on the laser power. In the SRS regime, the pumping photons are depleted in favor of the Stokes photons. This means that the scattered intensity at the pump frequency has to be reduced. Because we deal with the internal intensities, a change in the far-field signal at the zero Raman shift remains in question. We observe a barely perceptible nonlinear growth of the intensity at 0 cm^{-1}. The fitting of the experimental data with a function $I_P = aI_0 + bI_0^3$ yields the following ratio a/b = 175. The small value is caused by a contribution from the Rayleigh scattering. The observable amplification of the intensity at 0 cm^{-1} can be explained with the "induced" absorption of anti-Stokes photons which are reemitted at the pump frequency (Figure 1c). In other words, this phenomenon can be a signature of the IRS effect.[9,10] Indeed, the cubic nonlinearity drives the interaction between the anti-Stokes wave and the plasmon pump. The latter can be considered as a broadband continuum that is evidenced with the edge-stimulated photoluminescence in TiN thin films, as seen in Figure 5a.[37] Because we deal with the internal intensities, IRS is not straightforward effect to observe.

In summary, we conclude that nonlinear optical phenomena such as stimulated Raman emission (gain) and absorption (loss) effects can be observed in TiN plasmonic antennas exposed to cw laser irradiation with the intensity of 1 MW/cm^2. This antenna is fabricated on the refractory TiN thin film that is simultaneously plasmonic and Raman-gain medium. The total amplification of scattered localized light is produced due to three mechanisms. The first one is related to the edge-like nanoantenna that feeds the incident irradiation to make it localized and enhanced. The second mechanism results from a contribution occurring due to the formation of standing-wave resonances, and this is out of scope of this study. Finally, the third one is provided by the nonlinear Raman-gain medium in which stimulated SPPs are excited at both Stokes and anti-Stokes frequencies. One should emphasize that the effect in question occurs due to the near-field enhancement of attenuated plasmon polariton modes but not due to the Fabry-Pérot resonances. The findings presented in this Letter describe a novel stimulus for the development of ultracompact Raman lasers and amplifiers and biosensors.

AUTHOR INFORMATION

Corresponding Author

*E-mail: (S.S.K.) Sergey.Kharintsev@kpfu.ru.

ORCID

Sergey S. Kharintsev: 0000-0002-5788-3401

Sergei G. Kazarian: 0000-0003-1768-9134

Notes

The authors declare no competing financial interest.

ACKNOWLEDGMENTS

This work was financially supported by the Russian Foundation for Basic Research (No. 15-42-02339). The authors are grateful to D. Migunov and A. Dedkova (Moscow Institute for Electronic Technology, Russia) for their help in characterizing TiN thin films with scanning electron microscopy and spectroscopic ellipsometry. This work was done using equipment of Federal Center of Shared Equipment of Kazan Federal University and the Shared Center Facilities "MST&ECB" supported by Grant MSE Russia RFMEFI57816X0188. S.K.S. acknowledges the support from the subsidy allocated to Kazan Federal University for performing the state assignment in the area of scientific activities (Grant 3.2166.2017/4.6) and the Center for Excitonics, an Energy frontier Research Center funded by the U.S. Department of Energy under award DE-SC0001088.

REFERENCES

(1) Rong, H. S.; Xu, S. B.; Kuo, Y. H.; Sih, V.; Cohen, O.; Raday, O.; Paniccia, M. *Nat. Photonics* **2007**, *1*, 232−237.

(2) Liang, D.; Bowers, J. E. *Nat. Photonics* **2010**, *4*, 511−517.

(3) Homola, J. *Chem. Rev.* **2008**, *108*, 462−493.

(4) Stewart, M. E.; Anderton, C. R.; Thompson, L. B.; Maria, J.; Gray, S. K.; Rogers, J. A.; Nuzzo, R. G. *Chem. Rev.* **2008**, *108*, 494−521.

(5) Jiang, S.; Zhang, Y.; Zhang, R.; Hu, C. R.; Liao, M. H.; Luo, Y.; Yang, J. L.; Dong, Z. C.; Hou, J. G. *Nat. Nanotechnol.* **2015**, *10*, 865−869.

(6) Boyd, R. W. *Nonlinear Optics*; Academic Press: San Diego, 2008.

(7) Wang, C. S. *Phys. Rev.* **1969**, *182*, 482−494.

(8) Long, D. A. *The Raman Effect: A Unified Treatment of the Theory of Raman Scattering by Molecules*; Wiley: Chichester, 2002.

(9) Leites, D. A. *Russian Math. Surveys* **1980**, *35*, 1−64.

(10) Solli, D. R.; Koonath, P.; Jalali, B. *Phys. Rev. A: At., Mol., Opt. Phys.* **2009**, *79*, 053853.

(11) Kauranen, M.; Zayats, A. V. *Nat. Photonics* **2012**, *6*, 737−748.

(12) Razdolski, I.; Makarov, D.; Schmidt, O. G.; Kirilyuk, A.; Rasing, T.; Temnov, V. V. *ACS Photonics* **2016**, *3*, 179−183.

(13) Boltasseva, A.; Atwater, H. A. *Science* **2011**, *331*, 290−291.

(14) Zhu, C. J.; Ren, Y.; Zhao, X.; Huang, G. X.; Deng, L.; Hagley, E. W. *Appl. Phys. Lett.* **2014**, *104*, 203108.

(15) Ameling, R.; Langguth, L.; Hentschel, M.; Mesch, M.; Braun, P. V.; Giessen, H. *Appl. Phys. Lett.* **2010**, *97*, 253116.

(16) Naik, G. V.; Shalaev, V. M.; Boltasseva, A. *Adv. Mater.* **2013**, *25*, 3264−3294.

DOI: 10.1021/acs.nanolett.7b02252
Nano Lett. 2017, 17, 5533−5539

(17) Guler, U.; Boltasseva, A.; Shalaev, V. M. *Science* **2014**, *344*, 263−264.
(18) Jacob, Z.; Smolyaninov, I. I.; Narimanov, E. E. *Appl. Phys. Lett.* **2012**, *100*, 181105.
(19) Wu, H. Z.; Chou, T. C.; Mishra, A.; Anderson, D. R.; Lampert, J. K.; Gujrathi, S. C. *Thin Solid Films* **1990**, *191*, 55−67.
(20) Kinsey, N.; Syed, A. A.; Courtwright, D.; DeVault, C.; Bonner, C. E.; Gavrilenko, V. I.; Shalaev, V. M.; Hagan, D. J.; Van Stryland, E. W.; Boltasseva, A. *Opt. Mater. Express* **2015**, *5*, 2395−2403.
(21) Sutherland, R. L.; Mclean, D. G.; Kirkpatrick, S. *Handbook of Nonlinear Optics*; Marcel Dekker: New York, 2003.
(22) Chen, C. C.; Liang, N. T.; Tse, W. S.; Chen, I. Y.; Duh, J. G. *Chin. J. Phys.* **1994**, *32*, 205−210.
(23) Spengler, W.; Kaiser, R. *Solid State Commun.* **1976**, *18*, 881−884.
(24) Bernard, M.; Deneuville, A.; Thomas, O.; Gergaud, P.; Sandstrom, P.; Birch, J. *Thin Solid Films* **2000**, *380*, 252−255.
(25) Kharintsev, S.; Alekseev, A.; Vasilchenko, V.; Kharitonov, A.; Salakhov, M. *Opt. Mater. Express* **2015**, *5*, 2225−2230.
(26) Bozhevolnyi, S. I.; Sondergaard, T. *Opt. Express* **2007**, *15*, 10869−10877.
(27) Sondergaard, T.; Bozhevolnyi, S. I. *Opt. Express* **2007**, *15*, 4198−4204.
(28) Sondergaard, T.; Beermann, J.; Boltasseva, A.; Bozhevolnyi, S. I. *Phys. Rev. B: Condens. Matter Mater. Phys.* **2008**, *77*, 115420.
(29) Della Valle, G.; Sondergaard, T.; Bozhevolnyi, S. I. *Opt. Express* **2008**, *16*, 6867−6876.
(30) Novotny, L. *Phys. Rev. Lett.* **2007**, *98*, 266802.
(31) Maier, S. A. *Plasmonics: Fundamentals and Applications*; Springer: New York, 2007.
(32) Solovan, M. N.; Brus, V. V.; Maryanchuk, P. D.; Fodchuk, I. M.; Lorents, V. M.; Sletov, A. M.; Sletov, M. M.; Gluba, M. *Opt. Spectrosc.* **2014**, *117*, 753−755.
(33) Kharintsev, S. S.; Fishman, A. I.; Kazarian, S. G.; Salakhov, M. Kh. *Phys. Rev. B: Condens. Matter Mater. Phys.* **2015**, *92*, 115113.
(34) Anderson, N.; Bouhelier, A.; Novotny, L. *J. Opt. A: Pure Appl. Opt.* **2006**, *8*, S227−S233.
(35) Spengler, W.; Kaiser, R.; Christensen, A. N.; Mullervogt, G. *Phys. Rev. B: Condens. Matter Mater. Phys.* **1978**, *17*, 1095−1101.
(36) Kharintsev, S. S.; Salakhov, M. K. *Spectrochim. Acta, Part A* **2004**, *60*, 2125−2133.
(37) Boyd, G. T.; Yu, Z. H.; Shen, Y. R. *Phys. Rev. B: Condens. Matter Mater. Phys.* **1986**, *33*, 7923−7936.

DOI: 10.1021/acs.nanolett.7b02252
Nano Lett. 2017, 17, 5533−5539